Journal of Solid State Electrochemistry
https://doi.org/10.1007/s10008-024-05855-0

ORIGINAL PAPER

Detection of prostate cancer using an electrochemical sensor integrated with molecular imprinting technology and ionic liquid: a novel approach

Ademar Wong[1,2] · Shakeel Zeb[1] · Anderson M. Santos[3] · Maria H. A. Feitosa[3] · Sabir Khan[4] · Fernando C. Moraes[3] · Maria D. P. T. Sotomayor[1]

Received: 2 February 2024 / Revised: 3 March 2024 / Accepted: 4 March 2024

Abstract
Carbon paste electrodes have been used for decades in electro-analytical screening, with numerous advancements in modifying electrochemical properties. Different materials have been utilized in various applications, encompassing electroanalytical techniques and healthcare sensing. The current research addresses the enhancement of the carbon paste electrode with ionic liquid and molecularly printed polymers for sensitive and selective detection of the sarcosine biomarker. The materials were characterized using their structural and morphological properties, and the roughness and surface area of the polymer were evaluated. The electrochemical response for sarcosine was obtained at a potential of 1.2 V by modifying the carbon paste electrode with ionic liquid and magnetic molecularly imprinted polymers (mMIPs). Under optimized conditions, the proposed method showed a concentration linear range of 2.0×10^{-7} to 1.04×10^{-4} mol L^{-1} and a low detection limit of 5.1×10^{-8} mol L^{-1}. Aiming to demonstrate the efficiency of the proposed sensor, tests with biological samples were performed. The results showed robust recovery of sarcosine, ranging between 96 to 104% at two different concentration levels, affirming the efficacy of this method in determining sarcosine.

Keywords Sarcosine · mMIP · Electrochemical sensor · Ionic liquid · Biological samples

Introduction

Prostate cancer is a malignant disease that affects men and is one of the main causes of morbidity and mortality. The serum prostate-specific antigen (PSA) test remains the standard for early detection and monitoring of prostate cancer. However, there is still a lack of biomarkers to identify the most aggressive forms of this cancer. Urine-based tests can serve clinical and mass screening purposes, providing predictive and prognostic information due to their non-invasive character. Protein, DNA, and RNA-based tests are the three main categories of urine-based diagnostics [1, 2]. It is known that sarcosine is an amino acid produced by the human body that is present in urine and muscles and that can be used in the diagnosis of prostate cancer [3]. Elevated concentrations of sarcosine have been found in invasive prostate cancer cell lines compared to normal prostate epithelial cells [4, 5]. To detect sarcosine, various methods are reported in the literature such as chromatographic [6], colorimetric [7], chemiluminescence [8], spectrophotometric [9], spectrometric and electrochemical [10], and electrochemical methods [11]. The pursuit to craft materials featuring highly selective polymeric receptors, engineered with artificial recognition sites displaying a preference for the targeted rebinding of molecules, has prompted the proposal to develop molecularly imprinted polymers (MIPs). MIPs are highly cross-linked three-dimensional polymer networks with selective properties produced by the polymerization of functional monomers and

✉ Ademar Wong
ademar.wong@unesp.br

1 Institute of Chemistry, São Paulo State University (UNESP), Araraquara, SP, Brazil

2 Toxicological Evaluation and Removal of Micropollutants and Radioactive Substances (INCT-DATREM), National Institute for Alternative Technologies of Detection, Araraquara, São Paulo 14801-970, Brazil

3 Department of Chemistry, Federal University of São Carlos (UFSCar), São Carlos, São Paulo 13560-970, Brazil

4 Santa Cruz State University (UESC), CEP, Rodovia Jorge Amado, Km 16, Bairro SalobrinhoIlhéus, Bahia 45662-900, Brazil

Published online: 26 March 2024

cross-linking reagents around a model molecule [12–14]. The combination of molecular imprinting technology with nanomaterials would produce a powerful analytical tool with all desirable properties while also exhibiting greater selectivity than common silica adsorbents [15, 16]. Thus, the development of electrochemical sensors modified with combined materials aims to achieve optimal results, with a lower limit of detection [17, 18].

Briefly, electroanalytical methods offer greater simplicity, fast analysis, good selectivity and sensitivity, and especially low cost of analyte detection in different sample matrices [19, 20]. With recent advances in the use of electrochemical sensors and biosensors, new methodologies involving electrode modification have been reported, such as the use of modified carbon paste electrodes. In this context, the use of ionic liquid (IL), whether as binders or modifiers, has made it possible to increase the analytical signal in the detection of analytes of interest [21, 22]. IL possesses favorable solubility and high viscosity, enabling seamless blending with other materials and filling interstitial spaces, thus improving conductivity and electron transfer [23, 24]. Several research groups have sought to develop sensitive and selective MIPs with other materials, such as carbon materials, metallic nanoparticles, ionic liquids, and other compounds for application in electrochemical sensors.

In this sense, this work proposes the synthesis, characterization, and application of new material based on magnetic nanoparticles coated with MIP and IL for sensitive and selective detection of the sarcosine molecule using electrochemical sensors.

Experimental

Reagents and apparatus

Sarcosine, 1-buthyl-3-methylimidazolium tetrafluoroborate (IL), $FeCl_3.6H_2O$, $FeCl_2.4H_2O$, allyl-alcohol, tetraethoxysilane (TEOS), fluorenylmethyl-chloroformate (FMOC-Cl), ascorbic acid, glucose, uric acid, and NH_4OH were acquired from Sigma-Aldrich. Ethanol, toluene, acetonitrile, methanol, acetic acid, mineral oil, NaCl, KCl, urea, Na_2CO_3, NaH_2PO_4, and Na_2HPO_4 were purchased from LAC. All the solutions were prepared using ultrapure water (Millipore Milli-Q), and the resistivity of water was greater than 18.2 MΩ cm.

The electrochemical measurements were performed using an Autolab potentiostat/galvanostat PGSTAT 128N (Metrohm-Autolab) controlled by NOVA 2.1 software. The experiments were conducted using a three-electrode electrochemical cell, which consisted of the following: a carbon paste electrode (CPE) used as the working electrode (diameter = 0.30 cm), platinum wire employed as a counter electrode, and Ag/AgCl (KCl 3.0 mol L^{-1}) employed as reference electrode.

The pH of the solutions was adjusted using a pH meter with a glass electrode combined with an external reference electrode Ag/AgCl (3.0 mol L^{-1} KCl) (Orion Expandable Ion Analyzer). The morphology of the materials was evaluated by field emission scanning electron microscopy using FEG/SEM, with an electron beam energy of 25 keV) in mode (Supra 35-VP, Carl Zeiss, Germany), operating at 5 kV. The samples were prepared using the same proportion of material of the carbon paste. An aliquot of 15 µL of each diluted suspension was dropped on a silicon plate and was left to dry for 6 h at room temperature.

Confocal analysis was made using a confocal optical microscope (LEXT OLS 4000) controlled by Olympus software. The samples were prepared using a clean rectangular glass plate, and a mass of 1.0 mg of mMIP and mNIP (magnetic non-molecular imprinted polymers) was weighed and added to a 5.0-mL flask. An amount of 100 µL of this suspension was added in a specific area of 1.0 cm × 1.0 cm using adhesive tape.

Brunauer–Emmett–Teller (BET) analysis was performed using the ASAP 2020 (Micrometrics) equipment. The textural parameters of the polymers, such as specific surface area (BET) and pore volume (PV) were calculated using adsorption–desorption isotherms with nitrogen gas.

Synthesis of modified magnetic nanoparticles

The magnetic nanoparticles were synthesized in three steps, such as (i) synthesis of magnetic nanoparticles, (ii) modification with TEOS, and (iii) silanization with MPS. Under an inert environment and with constant agitation, 40 mL of H_2O was used to dissolve the appropriate amount of $FeCl_3.6H_2O$ and $FeCl_2.4H_2O$. The reaction system was then treated with 10 mL of NH_4OH in a drop-by-drop way, while the reaction was kept at 80 °C for 30 min. To eliminate any unreacted compounds, the black Fe_3O_4 nanoparticle precipitate was magnetically separated and washed in deionized water before being dried in a vacuum [25]. The nanoparticles of Fe_3O_4 (300 mg) were first dispersed in 40 mL of ethanol (EtOH) and 4.0 mL of deionized water using ultra-sonication for 15 min, after which, 5 mL of NH_4OH and 2.0 mL of TEOS were added. At room temperature, the mixture was allowed to react for 12 h. After collecting via magnetic separation, the products were washed three times with deionized water before being vacuum-dried. Then, 250 mg of Fe_3O_4@SiO_2 nanoparticles were dispersed in 50 mL of anhydrous toluene containing 5.0 mL of 3-metacriloxipropiltrimetoxissilano (MPS), and the mixture was left to react for 12 h in a nitrogen atmosphere. The final product was then magnetically separated using an external magnet before being vacuum-dried [26].

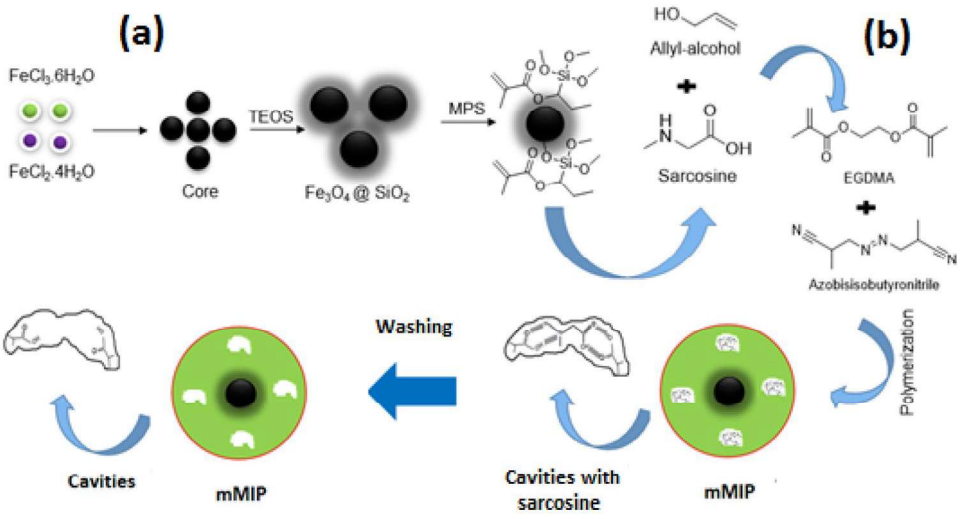

Scheme 1 The schematic representation of the formation of magnetic nanoparticles (**A**) and synthesis of mMIP (**B**) [28]

Synthesis of mMIP and mNIP

Polymerization of 1.0×10^{-3} molar sarcosine (SA) and 4.0×10^{-3} mol monomer Allyl alcohol in a total volume of 30 mL (24 mL water and 6.0 mL acetonitrile). The reaction system was agitated at 25 °C for 3 h, and then 100 mg of modified magnetic nanoparticles were added and agitated for 3 more hours. In addition, 20×10^{-3} molar of EGDMA and 0.084×10^{-3} mol of AIBN were introduced into the system, sonicated for 5 min in a nitrogen atmosphere, and then the reaction mixture was kept at 60 °C for 24 h while being shielded from oxygen by nitrogen gas [27]. Soxhlet extraction using methanol: acetic acid (9:1, v/v) as eluent was used to remove the template molecule after polymerization, and the eluent was changed every 12 h. The products (mMIPs) were then dried at 40 °C under a vacuum after completely removing the template molecule. In the same way, mNIPs, or magnetic non-molecular imprinted polymers, were synthesized in the absence of an analyte. The synthesis process of the magnetite (Fe_3O_4) and mMIP can be found in Scheme 1.

Preparation of the CPE modified with IL and mMIP

The modified working electrode (1.5 mm in diameter and 1.0 mm deep) was prepared using an amount of modified carbon paste with 15 mg of mMIP, 85 mg graphite, and 1.0 mL of ionic liquid (1.0 mg mL^{-1}). Initially, the graphite was mixed with the ionic liquid and dried at a temperature of 25 °C for 4 h. After, the mMIP was added, and the materials were subjected to homogenization for 5 min, and then mineral oil was added to obtain the modified carbon paste.

The electrode surface was prepared by adding a quantity of carbon paste to fill the electrode cavity and then polished with a clean sheet of paper before carrying out electrochemical measurements. The same procedure was used to renew the surface. The proportion of the mass of mMIP and graphite powder and mMIP tested was 10/90, 15/85, 20/80, and 25/75 mg being used in the procedure of a mortar and pestle, and the ionic liquid solutions tested were 0.5, 1.0, and 1.5 mg of IL in a volume of 1.0 mL of solution.

Preparation of biological samples

Synthetic urine samples were prepared by mixing the following substances in a 25-mL flask containing 49 mmol L^{-1} NaCl, 20 mmol L^{-1} KCl, 10 mmol L^{-1} $CaCl_2$, 15 mmol L^{-1} KH_2PO_4, 18 mmol L^{-1}, NH_4Cl, and 18 mmol L^{-1} urea [29]. The ultrapure water was added to complete the volume. The human serum sample was prepared using 2.0 mL of serum samples in a 25 mL volumetric flask containing 23 mL of ultrapure water.

Aliquots of 250 µL of the samples were tested using DPV-based electrochemical experiments. The results obtained showed that there was no electrochemical signal of sarcosine. The samples were spiked with sarcosine using two concentration levels (5.0×10^{-7} mol L^{-1} and 5.0×10^{-6} mol L^{-1}), and the stock solution was diluted 50 times.

HPLC–UV analysis and sarcosine derivatization

The derivatization reaction of sarcosine was made according to a study by Hottes et al. [30]. The standard solution of sarcosine was prepared at different levels of concentration using the ratio 1:2 (m/m) of sarcosine and 9-fluorenylmethyl-chloroformate (FMOC-Cl). The chemical reaction was performed using the Britton-Robinson buffer solution (pH = 9.0)/acetonitrile in the ratio 1:1 v/v in an optimized reaction time of 30 min [31, 32]. After this step, the samples were prepared and analyzed in high-performance liquid chromatography with a UV detector (HPLC–UV).

The HPLC–UV analysis was performed using a Shimadzu HPLC 20A, equipped with an automatic injector

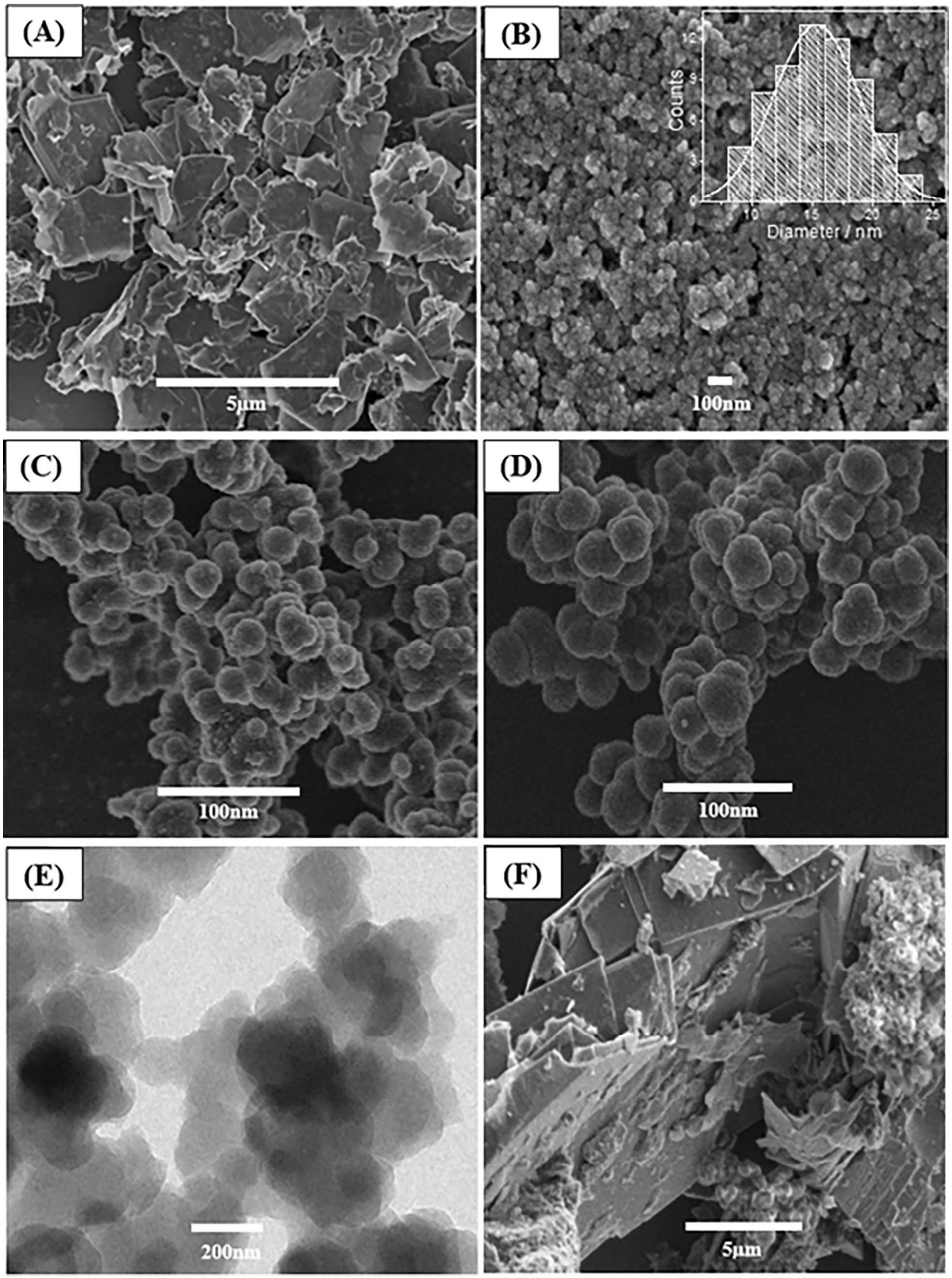

Fig. 1 Morphological characterization of the materials: **A** graphite, **B** graphite and IL, **C** mMIP, **D** mNIP, **E** TEM image of mMIP and **F** graphite and **F** IL and mMIP

(model SIL-20A), quaternary pump, degasser system (model DGU-20A5), and UV detector (model SPD-20A). Chromatographic separation was performed using a reversed-phase C18 column (4.6 × 250 mm, 5 µm) Shim-pack CLC, Shimadzu. The mobile phase was composed of a mixture of 1.0×10^{-3} mol L^{-1} phosphate buffer (pH = 5.0) and acetonitrile in the volumetric ratio of 50:50 *v*/*v*, respectively. The flow rate was adjusted to 1.0 mL min^{-1}, the detector was operated at the wavelength of 206 nm, and the analysis time was 15 min for each sample [33].

Results and conclusion

Morphological characterization and confocal analysis

The morphological characterization of the synthesized polymers was evaluated by scanning electron microscopy (SEM). Figure 1A shows the morphology of graphite, which is arranged in irregular plates of different sizes. The micrographs in Fig. 1B depict magnetic nanoparticles with an average diameter of 15 nm. A diameter of 285 nm was produced by modifying the magnetic nanoparticles. Figure 1C, D shows the morphological aspects of mMIP and mNIP, respectively. The formation of a core@shell is known to occur when magnetic nanoparticles are coated with MIP and NIP. The TEM image confirms that mMIP was formed on the magnetic nanoparticles with the presence of a lighter and a darker region (Fig. 1E). The FEG-SEM images cannot be distinguished because the cavities formed from mMIP are at the molecular level. Figure 1F makes it possible to visualize two distinct phases, with large plates belonging to graphite and regular-sized spherical nanoparticles belonging to polymers. When IL was mixed with graphite, no morphological difference was observed due to the adsorption that occurred.

FTIR, BET, and confocal analysis of the polymers

The roughness of the polymers synthesized was obtained using the Olympus FV3000 confocal laser scanning microscope. Figure 2A, B shows a 3D image of mMIP and mNIP deposited on a glass plate. The roughness value (R_a) found was 4.1 µm for mMIP and 1.2 mNIP, indicating an increase of 3.4 times. This information was expected because mMIP has selective cavities that promote greater roughness. The specific surface values and pore volume for mNIP were 18.2 m^2 g^1 and 0.08 cm^3g^{-1}, while for mMIP were 32.5 m^2 g^1 and 0.14 cm^3g^{-1}, as determined by BET evaluation.

Fourier transform infrared (FTIR) spectroscopy was employed to examine the samples of the chemical groups of the polymers (mMIP and MNIP). Figure 2C illustrates the

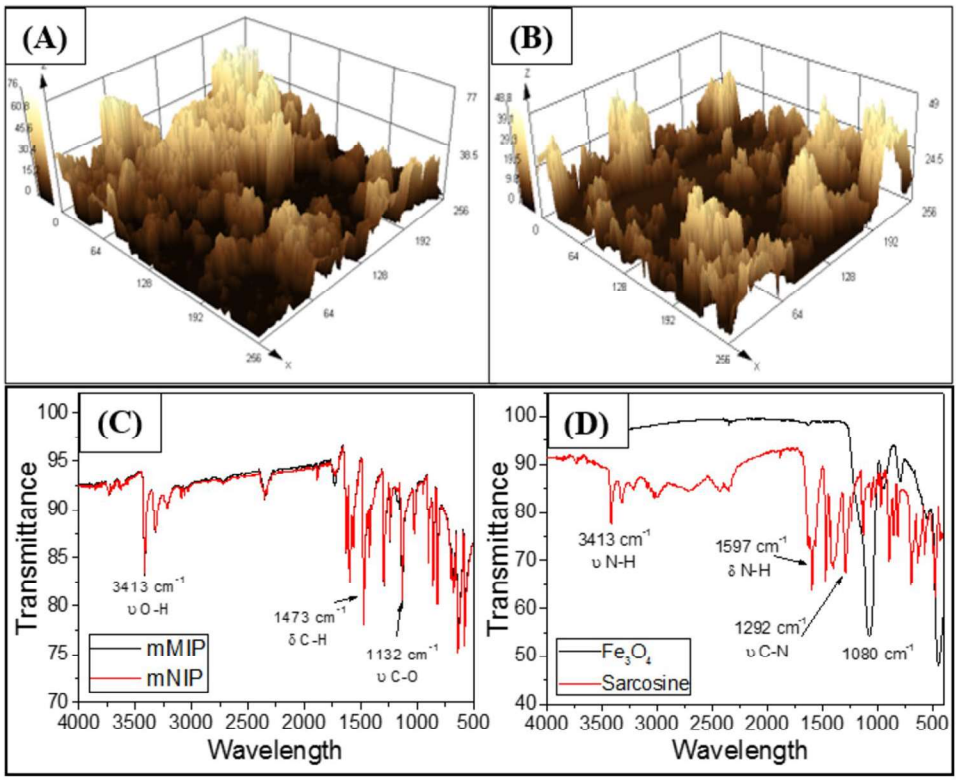

Fig. 2 Confocal image of mMIP (**A**) and mNIP (**B**) and FTIR analysis of mMIP (**C**) and mNIP (**D**)

infrared (IR) spectra of the molecularly imprinted polymer (MIP) and non-imprinted polymer (NIP). It is noteworthy that their main composition primarily consists of the EGDMA as a cross-linker and the allyl alcohol as a functional monomer, elucidating the bands associated with the groups present in these molecules. The band at 3413 cm^{-1} corresponds to the O–H stretching in allyl alcohol, as reported in the literature. The band at 1473 cm^{-1} is associated with the C-H bending present in both allylic alcohol and EGDMA. Lastly, the band at 1132 cm^{-1} is attributed to the C-O stretching of the ester group, which is present in EGDMA. Figure 2D shows the infrared spectrum of the sarcosine molecule and the Fe_3O_4. For the sarcosine molecule, three significant bands are evident from the figure. The first, with a wave number of 3413 cm^{-1}, corresponds to the N–H stretching of the amine present in the molecule. The band at 1597 cm^{-1} also relates to the N–H bond, specifically its bending vibration. The band highlighted at 1292 cm^{-1} corresponds to the stretching of the C–N bond in the same amino group, while in the Fe_3O_4 sample, a large characteristic peak at 1080 cm^{-1} was observed, which corresponds to the Fe–O stretching vibration in tetrahedral sites [34].

Optimization of the experimental conditions

The electrochemical behavior of sarcosine in different electrolytes (phosphate, TRIM, acetate, and Britton-Robinson buffers) was investigated by DPV. The results revealed phosphate buffer electrolytes showed the best oxidation current. Therefore, this buffer was chosen in the subsequent electrochemical analyses.

Next, the influence of pH on the electrochemical oxidation of sarcosine was studied by the DPV technique in a range of a pH of 5.0 to 10.0, using a phosphate buffer solution. As can be seen, the reduction of the hydrogen ionic concentration of the electrolyte causes a shift in peak potential for sarcosine oxidation towards more negative values (Fig. 3). This is a consequence of deprotonation during the oxidation process, which is facilitated at higher pH values. The plot of I_{pa} *vs.* pH for sarcosine shows that the anodic peak current increases in the pH range of 5.0 to 9.0, reaching a maximum value at pH 9.0. Therefore, pH 9.0 was chosen as the optimal value.

In addition, it was found that the sensor did not influence the ability of the electrochemical signal of sarcosine in the DPV analyses.

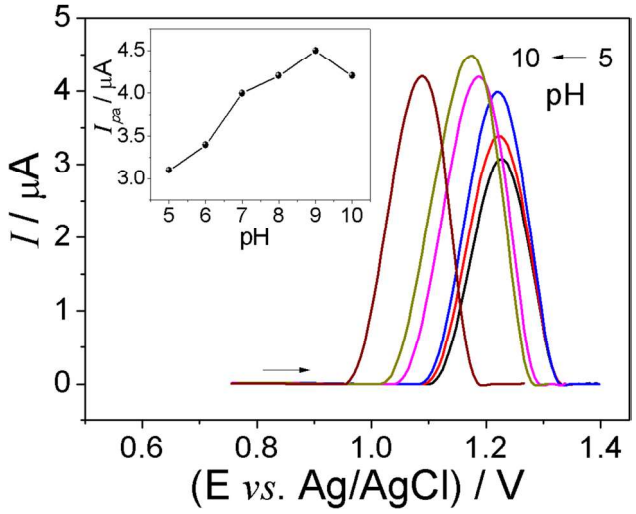

Fig. 3 Effect of pH on the electrochemical response of the mMIP-IL/CPE sensor in 0.10 mol L^{-1} phosphate buffer using the DPV technique. Analysis conditions: scan rate = 50 mV s^{-1}, step potential = 5 mV, pulse amplitude = 75 mV, and sarcosine concentration = 5.0×10^{-5} mol $L.^{-1}$

Electrochemical profile of sarcosine

The electrochemical profile of the sarcosine was evaluated using different electrodes with the differential pulse voltammetry (DPV) technique in a potential range from 0 to + 1.4 V. In these experiments, a concentration of sarcosine was added in an electrochemical cell, and the electrochemical response was obtained for the electrodes as shown in Fig. 4. The mMIP-IL/CPE reveals well-defined irreversible oxidation peaks of the sarcosine at + 1.2 V showing the best analytical signal when compared to IL/CPE and CPE using 0.1 mol L^{-1} of phosphate buffer solution at pH 9.0 (Fig. 4A, B). Compared to the ionic liquid and TiO_2 nanoparticles modified sensor proposed by Bahrami et al., the peak potential was similar in the sarcosine oxidation [35].

Effect of scan rate on the peak currents and potentials

To study the mass transport kinetics of the analyte in the bulk solution to the surface of the electrode, the scan rate study was performed with the electrode modified by cyclic voltammetry. Figure 5 shows the cyclic voltammetry response of the modified electrode in a potential range of − 0.7 to 1.5 V. The anodic peak and redox potentials, respectively, increased and significantly shifted with the scan rate increased from 20 to 300 mV/s in the presence of 5.0×10^{-4} mol L^{-1} sarcosine solution using 0.10 mol L^{-1} phosphate buffer at pH 9.0. From the current values obtained in this study, it was possible to construct the anodic peak current graph as a function of υ and $\upsilon^{1/2}$. Analyzing the curve of the peak current (I_{pa}) against the square root of scan rate ($\upsilon^{1/2}$) and scan rate (υ) can be seen in the linear regression equation; the correlation coefficient (R^2) of I_{pa} *vs.* $\upsilon^{1/2}$ plot was 0.975, while I_{pa} *vs.* υ plot was 0.999. This suggests that the transport of the analyte to the electrode surface is controlled by adsorption.

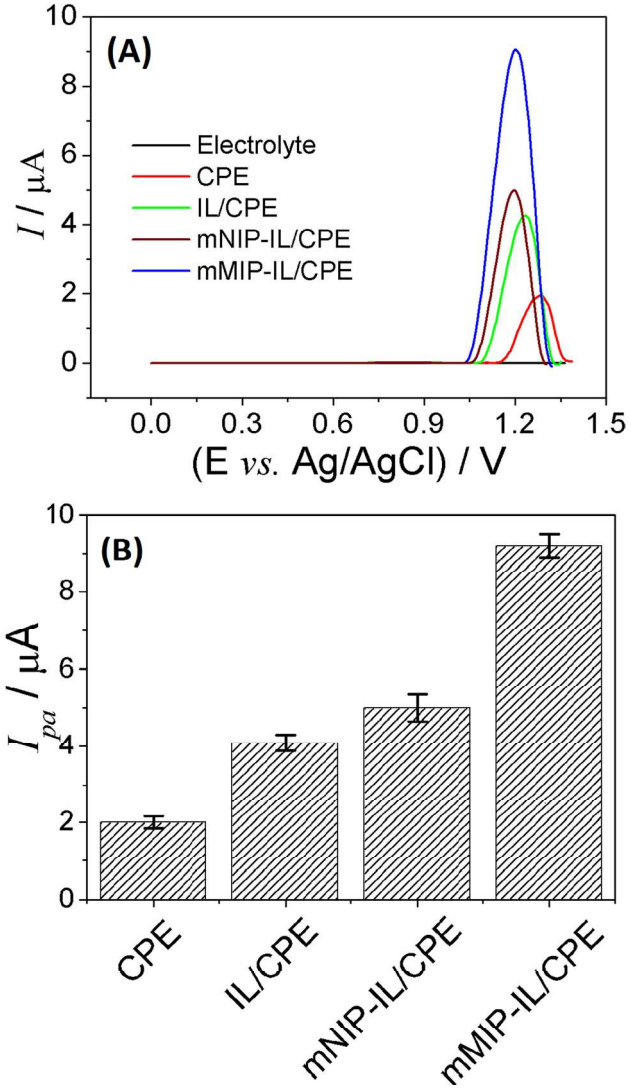

Fig. 4 Profile electrochemical of the studied electrodes by DPV (**A**) and error bar plot (**B**). Analysis conditions: $\upsilon = 50$ mV s^{-1}, $\Delta E = 5$ mV, pulse amplitude = 75 mV, and sarcosine concentration = 1.5×10^{-4} mol $L.^{-1}$

Aiming to find the number of electrons in the electrochemical reaction of sarcosine in basic solution, the Laviron equation was utilized (Eq. 1).

$$E_P = E^{\circ'} + \left(\frac{2,303 \,.\, R \,.\, T}{\alpha.n.F}\right) \cdot \log\left(\frac{R \,.\, T \,.\, K^{\circ}}{\alpha.n.F}\right) + \left(\frac{2,303 \,.\, R \,.\, T}{\alpha.n.F}\right) \cdot \log\ \upsilon \quad (1)$$

Where $R = 8.314$ J mol^{-1} K^{-1}, $T = 298$ K, α = charge transfer coefficient, $F = 96.485$ C mol^{-1}, and n = electron number.

A slope of 0.059 was found by analyzing the linear regression of the curve E_p *vs.* log υ. In this sense, it was possible to find the value of αn that was 0.94 and consider $\alpha = 0.5$

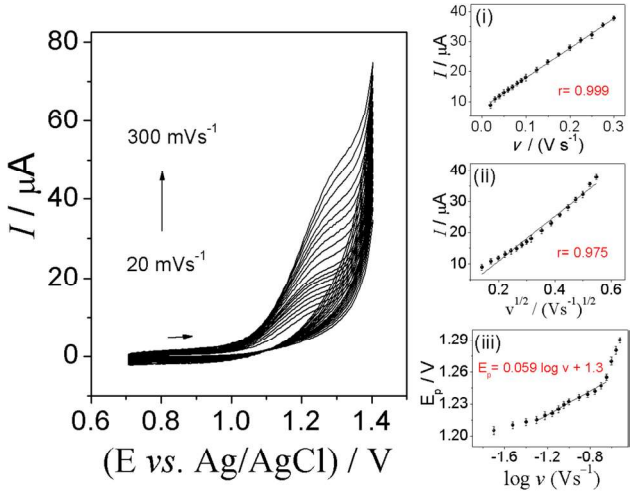

Fig. 5 Cyclic voltammograms recorded at different scan rates using the mMIP-IL/CPE for 5.0×10^{-4} mol L^{-1} sarcosine in phosphate buffer at pH = 9.0. Insets: (i) I_{pa} *vs.* υ, (ii) I_{pa} *vs.* $\upsilon^{1/2}$, and (iii) E_p *vs.* log υ

for the irreversible redox system. The electron number value calculated was 2 electrons. Scheme 2 makes it possible to visualize the electrochemical reaction of sarcosine occurring in two steps, involving one electron each.

Sarcosine determination by DPV method

The determination of sarcosine was performed using the DPV technique in a phosphate buffer solution (pH = 9.0). Under the best-tested analysis conditions (Table S1), the proposed method showed an analytical curve with a linear response in the concentration range of 2.0×10^{-7} to 1.04×10^{-4} mol L^{-1} and a limit of detection of 5.1×10^{-8} mol L^{-1} (calculated using $3 \times SD/m$, where SD is the standard deviation for ten blank solution measurements ($n = 10$), and m is the analytical sensitivity) (Fig. 6).

A comparison of the performance of mMIP-IL/CPE with other studies reported in the literature is shown in Table 1 [8, 35–39]. All of them have some advantages and limitations that make this sensor highly promising, whether in detection limit, linear response range, repeatability, and mainly low cost.

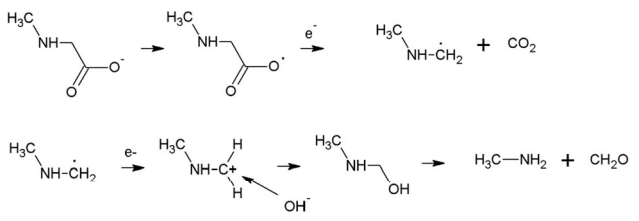

Scheme 2 The proposed mechanism of sarcosine electro-oxidation in basic solution [35]

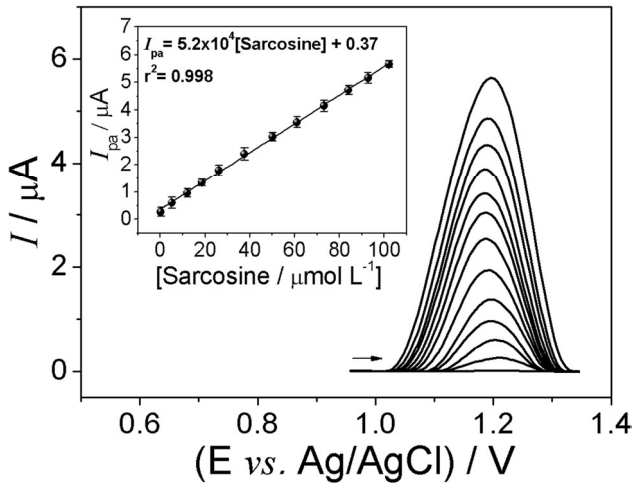

Fig. 6 DPV analysis of sarcosine using 0.10 mol L^{-1} phosphate buffer solution at pH 9.0. Analysis conditions: $\upsilon = 50$ mV s^{-1}, $\Delta E = 5$ mV, pulse amplitude = 75 mV

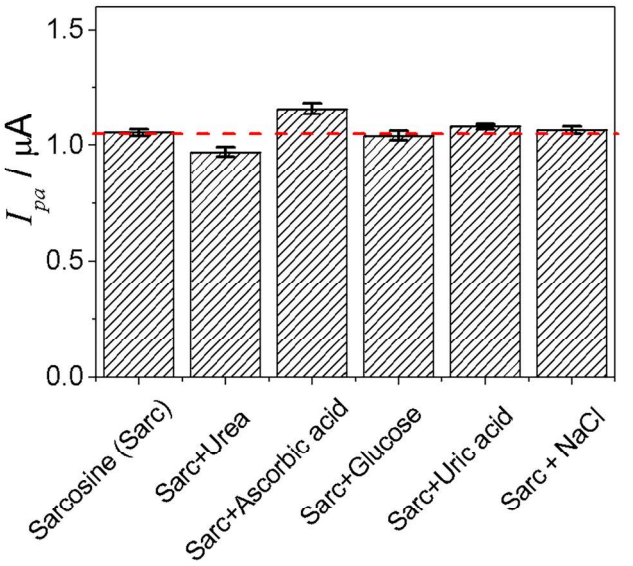

Fig. 7 Interferent study by DPV using mMIP-IL/CPE sensor. Analysis conditions: scan rate = 50 mV s^{-1}, step potential = 5 mV, pulse amplitude = 75 mV, and sarcosine and interferent concentration = 2.0×10^{-5} mol $L.^{-1}$

Repeatability and interference studies

The repeatability of the mMIP-IL/CPE sensor was studied by the DPV method using 2.5×10^{-5} mol L^{-1} sarcosine standard. To the DPV measurements ($n = 15$) were performed for each concentration was obtained and the relative standard deviations (RSD) less 5.0% demonstrating the precision and stability of the response of the proposed sensor (Fig. S1, Supplementary Material).

To evaluate the efficacy of the mMIP-IL/CPE in determining sarcosine, a study of interferences found in the biological matrix was conducted in connection to the interferent test. The interferents were urea, ascorbic acid, glucose, uric acid, and NaCl in the molar ratio 1:1, and the results showed no interference in the electrochemical signal of sarcosine (Fig. 7 and Supplementary Material, Fig. S2).

Application in biological samples

The proposed sensor was tested in synthetic biological samples to confirm their applicability and reliability. The percentage of recovery and relative standard deviation were calculated according to Table 2. The recoveries near 100% of the samples indicated that the proposed method

Table 1 Comparison analytical of the mMIP-IL/CPE sensor obtained in the determination of sarcosine with other studies reported in the literature

Electrode	Method	Linear range (mol L^{-1})	LOD (mol L^{-1})	Reference
Ni-1/GCE[a]	DPV	1.0×10^{-4} to 1.0×10^{-3}	-	[8]
AuPt-PPy/GR/GCE[b]	DPV	2.5×10^{-6} to 6.0×10^{-4}	0.7×10^{-6}	[35]
TiO_2/IL/CPE[c]	DPV	1.0×10^{-4} to 1.0×10^{-3}	8.0×10^{-5}	[36]
MWCNT/Nafion®/$Ni(OH)_2$/SPCE[d]	CV	3.2×10^{-6} to 2.5×10^{-5}	0.96×10^{-6}	[37]
CHIT/CuNPs/c-MWCNT/Au[e]	CV	0.1×10^{-6} to 1.0×10^{-4}	0.1×10^{-12}	[38]
SOxNPs/AuE	Amperometry	0.1×10^{-6} to 1.0×10^{-4}	1.0×10^{-8}	[39]
mMIP-IL/CPE	DPV	2.0×10^{-7} to 1.04×10^{-4}	5.1×10^{-8}	**This work**

[a]Ni metal–organic framework based on 2.20-Biphenyldicarboxylic, 4.40- bipyridine-based GCE

[b]Glassy carbon electrode (GCE) was modified with a graphene-chitosan (GR) composite and further modified with gold-platinum bimetallic nanoparticle

[c]Carbon paste electrode modified with TiO_2 nanoparticles in 1-butyl-3-methylimidazolium tetrafluoroborate ionic liquid

[d]MWCNT/Nafion®/$Ni(OH)_2$-modified screen-printed electrode

[e]Sarcosine oxidase/chitosan/CuNPs/c-MWCNT/Au electrode

Table 2 Application of mMIP-IL/CPE sensor in biological samples

Samples	[Sarcosine] / mol L^{-1}			Recovery (Sensor, %)**	Relative error (%)***
	Added	Found*	Comparative method*		
Synthetic urine	5.0×10^{-7}	$(5.2\pm0.3)\times10^{-7}$	$(5.0\pm0.1)\times10^{-7}$	104	+4.0
	5.0×10^{-6}	$(5.0\pm0.2)\times10^{-6}$	$(4.8\pm0.1)\times10^{-6}$	100	+4.2
Serum	5.0×10^{-7}	$(4.8\pm0.2)\times10^{-7}$	$(4.9\pm0.1)\times10^{-7}$	96.0	−2.0
	5.0×10^{-6}	$(4.9\pm0.3)\times10^{-6}$	$(5.0\pm0.1)\times10^{-6}$	98.0	−2.0

*Average of 3 measured concentrations

**Recovery percentage = [Found] / [Added] × 100

***Relative error = [(Proposed method − Comparative method) / (Comparative method)] × 100

can be successfully applied in the detection of sarcosine in biological samples. When comparing the results with the electrochemical sensor and HPLC–UV, the results showed that both procedures provided very consistent measurements, with a relative error of ± 4.0%. By applying the paired *t*-test, it was possible to find a $t_{experimental}$ value = 5.5 which was 2.3 times lower than the $t_{theoretical}$ value = 12.7, demonstrating the two methods were not statistically different (up to a confidence level of 95%). The chromatogram and analytical curve obtained from the derivatization reaction with FMOC-Cl can be viewed in the supplementary material, Fig. S3.

Conclusion

The modification of the carbon paste electrode with IL and mMIP improves the analytical signal, allowing an excellent catalytic activity towards the oxidation of sarcosine and a better detectability of sarcosine in biological samples. The mMIP-IL/CPE electrode demonstrated exceptional performance, low limited detection, rapid detection, and inexpensive cost while achieving satisfactory recoveries ranging from 96 to 104%. The proposed sensor allows for the detection of sarcosine with high sensitivity, affordability, and applicability in monitoring sarcosine in prostate cancer patients. The suggested method enables further advancements in the design of novel sensors to enhance human health quality affordably.

Supplementary Information The online version contains supplementary material available at https://doi.org/10.1007/s10008-024-05855-0.

Funding The authors gratefully acknowledge the financial assistance granted by PROPe-Unesp edital no. 13/2022), and the National Institute for Alternative Technologies of Detection, Toxicological Evaluation and Removal of Micropollutants and Radioactive Substances, INCTDATREN (FAPESP #2014/50945–4; CNPq #465571/2014–0) is acknowledged for the main technological support given to this work. This study was financed in part by the Coordination for the Improvement of Higher Education Personnel-Brazil (CAPES)-Finance Code 001. The authors gratefully acknowledge the financial support granted by FAPESP (grant no. 2022/03553–0 and 2022/05454–9).Fundação de Amparo à Pesquisa do Estado de São Paulo, 2022/03553-0, Maria D. P. T. Sotomayor, Pro-Reitoria de Pesquisa, Universidade de São Paulo, edital 13/2023, Ademar Wong.

Declarations

Competing interests The authors declare no competing interests.

References

1. Atieh Z, Allouche AR, Lazariev A et al (2010) DFT calculations of 1H chemical shifts, simulated and experimental NMR spectra for sarcosine. Chem Phys Lett 492:297–301. https://doi.org/10.1016/j.cplett.2010.04.054
2. Sreekumar A, Poisson LM, Rajendiran TM et al (2009) Metabolomic profiles delineate potential role for sarcosine in prostate cancer progression. Nature 457:910–914. https://doi.org/10.1038/nature07762
3. Cernei N, Heger Z, Gumulec J et al (2013) Sarcosine as a potential prostate cancer biomarker-a review. Int J Mol Sci 14:13893–13908. https://doi.org/10.3390/ijms140713893
4. Koutros S, Meyer TE, Fox SD et al (2013) Prospective evaluation of serum sarcosine and risk of prostate cancer in the prostate, lung, colorectal and ovarian cancer screening trial. Carcinogenesis 34:2281–2285. https://doi.org/10.1093/carcin/bgt176
5. Molter CW, Muszynski EF, Tao Y et al (2022) Prostate cancer cells of increasing metastatic potential exhibit diverse contractile forces, cell stiffness, and motility in a microenvironment stiffness-dependent manner. Front Cell Dev Biol 10:1–13. https://doi.org/10.3389/fcell.2022.932510
6. Jiang Y, Cheng X, Wang C, Ma Y (2010) Quantitative determination of sarcosine and related compounds in urinary samples by liquid chromatography with tandem mass spectrometry. Anal Chem 82:9022–9027. https://doi.org/10.1021/ac1019914
7. Zhong Q, Qin X, Yuan C et al (2021) Colorimetric determination of sarcosine in human urine with enzyme-like reaction mediated Au nanorods etching. Microchem J 165:106120. https://doi.org/10.1016/j.microc.2021.106120
8. Jing Y, Hu Y, He Y et al (2023) Novel chemiluminescence sensing for the visual detection of sarcosine based upon an iron-based metal–organic gel with peroxidase-like activity. Anal Lett 57:92–102. https://doi.org/10.1080/00032719.2023.2195187
9. Uhlirova D, Stankova M, Docekalova M et al (2018) A rapid method for the detection of sarcosine using SPIONs/Au/CS/SOX/NPs for prostate cancer sensing. Int. J. Mol. Sci. 19:3722. https://doi.org/10.3390/ijms19123722
10. Cernei N, Zitka O, Ryvolova M et al (2012) Spectrometric and electrochemical analysis of sarcosine as a potential prostate

carcinoma marker. Int. J. Electrochem. Sci. 7:4286–4301. https://doi.org/10.1016/s1452-3981(23)19538-1
11. Lin S, Wang Y, Zhang C et al (2021) Electrochemical detection of sarcosine and supercapacitor based on a new Ni–metal-organic framework electrode material. Crystals 11:1036. https://doi.org/10.3390/cryst11091036
12. Sajini T, Mathew B (2021) A brief overview of molecularly imprinted polymers: highlighting computational design, nano and photo-responsive imprinting. Talanta Open 4:100072. https://doi.org/10.1016/j.talo.2021.100072
13. Vasapollo G, Del SR, Mergola L et al (2011) Molecularly imprinted polymers: present and future prospective. Int J Mol Sci 12:5908–5945. https://doi.org/10.3390/ijms12095908
14. Belbruno JJ (2018) Molecularly imprinted polymers. Chem Rev 119:94–119. https://doi.org/10.1021/acs.chemrev.8b00171
15. Fresco-Cala B, Batista AD, Cárdenas S (2020) Molecularly imprinted polymer micro- and nano-particles: a review. Molecules 25:1–22. https://doi.org/10.3390/molecules25204740
16. Santos AM, Wong A, Prado TM et al (2021) Voltammetric determination of ethinylestradiol using screen-printed electrode modified with functionalized graphene, graphene quantum dots and magnetic nanoparticles coated with molecularly imprinted polymers. Talanta 224:121804. https://doi.org/10.1016/j.talanta.2020.121804
17. Irshad M, Iqbal N, Mujahid A et al (2013) Molecularly imprinted nanomaterials for sensor applications. Nanomaterials 3:615–637. https://doi.org/10.3390/nano3040615
18. Elugoke SE, Adekunle AS, Fayemi OE et al (2021) Molecularly imprinted polymers (MIPs) based electrochemical sensors for the determination of catecholamine neurotransmitters – review. Electrochem Sci Adv 1:1–43. https://doi.org/10.1002/elsa.202000026
19. Baranwal J, Barse B, Gatto G et al (2022) Electrochemical sensors and their applications: a review. Chemosensors 10:363. https://doi.org/10.3390/chemosensors10090363
20. Stradiotto NR, Yamanaka H, Zanoni MVB (2003) Electrochemical sensors: a powerful tool in analytical chemistry. J Braz Chem Soc 14:159–173. https://doi.org/10.1590/S0103-50532003000200003
21. Kaur H, Siwal SS, Chauhan G et al (2022) Recent advances in electrochemical-based sensors amplified with carbon-based nanomaterials (CNMs) for sensing pharmaceutical and food pollutants. Chemosphere 304:135182. https://doi.org/10.1016/j.chemosphere.2022.135182
22. Kour R, Arya S, Young S-J et al (2020) Review—recent advances in carbon nanomaterials as electrochemical biosensors. J Electrochem Soc 167:037555. https://doi.org/10.1149/1945-7111/ab6bc4
23. Ma X, Yu J, Hu Y et al (2023) Ionic liquid/poly(ionic liquid)-based electrolytes for lithium batteries. Ind Chem Mater 1:39–59. https://doi.org/10.1039/d2im00051b
24. Singh VV, Nigam AK, Batra A et al (2012) Applications of ionic liquids in electrochemical sensors and biosensors. Int J Electrochem 2012:1–19. https://doi.org/10.1155/2012/165683
25. Josefina R, Sánchez U, Khan S et al (2015) Magnetically separable polymer (Mag-MIP) for selective analysis of biotin in food samples. FOOD Chem 1:460–467. https://doi.org/10.1016/j.foodchem.2015.05.129
26. Ariani MD, Zuhrotun A, Manesiotis P, Hasanah AN (2022) Magnetic molecularly imprinted polymers: an update on their use in the separation of active compounds from natural products. Polymers (Basel) 14:1389. https://doi.org/10.3390/polym14071389
27. Diniz KM, Tarley CRT (2015) Speciation analysis of chromium in water samples through sequential combination of dispersive magnetic solid phase extraction using mesoporous amino-functionalized Fe3O4/SiO2 nanoparticles and cloud point extraction. Microchem J 123:185–195. https://doi.org/10.1016/j.microc.2015.06.011
28. Sheydaei O, Khajehsharifi H, Rajabi HR (2020) Rapid and selective diagnose of Sarcosine in urine samples as prostate cancer biomarker by mesoporous imprinted polymeric nanobeads modified electrode. Sensors Actuators, B Chem 309:127559. https://doi.org/10.1016/j.snb.2019.127559
29. Laube N, Mohr B, Hesse A (2001) Laser-probe-based investigation of the evolution of particle size distributions of calcium oxalate particles formed in artificial urines 233:367–374
30. Hottes E, Santos CRGR, de Souza HJM, et al (2021) Studies using hplc-pda in gabapentin N-derivatization reactions with 9-fluorenylmethyl chloroformate (FMOC-CL). Quim Nova 44:4. https://doi.org/10.21577/0100-4042.20170718
31. Catrinck TCPG, Dias A, Aguiar MCS et al (2014) A simple and efficient method for derivatization of glyphosate and AMPA using 9-fluorenylmethyl chloroformate and spectrophotometric analysis. J Braz Chem Soc 25:1194–1199. https://doi.org/10.5935/0103-5053.20140096
32. Zelenkova NF, Vinokurova NG, Leontievskii AA (2010) Determination of amine-containing phosphonic acids and amino acids as dansyl derivatives. J Anal Chem 65:1143–1147. https://doi.org/10.1134/S1061934810110092
33. Chung TC, Te LC, Kou HS, Wu HL (2015) High-performance liquid chromatographic analysis of sarcosine as a fluorescent levofloxacin derivative. J Chromatogr Sci 53:1310–1315. https://doi.org/10.1093/chromsci/bmv010
34. López R, Khan S, Torres SE et al (2023) Synthesis and characterization of magnetic molecularly imprinted polymer for the monitoring of amoxicillin in real samples using the chromatographic method. Magnetochemistry 9:92. https://doi.org/10.3390/magnetochemistry9040092
35. Bahrami H, Mousavi M, Maghsoudi S (2021) Sensitive voltammetric method for rapid determination of sarcosine as a new biomarker for prostate cancer using a TiO2 nanoparticle/ionic liquid modified carbon paste electrode. Russ J Electrochem 57:149–158. https://doi.org/10.1134/S1023193521020099
36. Liu T, Fu B, Chen J, Li K (2019) An electrochemical sarcosine sensor based on biomimetic recognition. Microchim Acta 186:1–8. https://doi.org/10.1007/s00604-019-3240-0
37. de Cássia MJ, da Rocha LR, Capelari TB et al (2020) Design and performance of novel molecularly imprinted biomimetic adsorbent for preconcentration of prostate cancer biomarker coupled to electrochemical determination by using multi-walled carbon nanotubes/Nafion®/Ni(OH)2-modified screen-printed electrode. J Electroanal Chem 878:114582. https://doi.org/10.1016/j.jelechem.2020.114582
38. Narwal V, Kumar P, Joon P, Pundir CS (2018) Fabrication of an amperometric sarcosine biosensor based on sarcosine oxidase/chitosan/CuNPs/c-MWCNT/Au electrode for detection of prostate cancer. Enzyme Microb Technol 113:44–51. https://doi.org/10.1016/j.enzmictec.2018.02.010
39. Kumar P, Narwal V, Jaiwal R, Pundir CS (2018) Construction and application of amperometric sarcosine biosensor based on SOxNPs/AuE for determination of prostate cancer. Biosens Bioelectron 122:140–146. https://doi.org/10.1016/j.bios.2018.09.003